AIP ADVANCES **5**, 087134 (2015)

Low contact resistance in epitaxial graphene devices for quantum metrology

Tom Yager,[1,a] Arseniy Lartsev,[1] Karin Cedergren,[2] Rositsa Yakimova,[3] Vishal Panchal,[4] Olga Kazakova,[4] Alexander Tzalenchuk,[4,5] Kyung Ho Kim,[6] Yung Woo Park,[6,a] Samuel Lara-Avila,[1] and Sergey Kubatkin[1]

[1]*Department of Microtechnology and Nanoscience, Chalmers University of Technology Göteborg, S-412 96, Sweden*
[2]*School of Physics, University of New South Wales, Sydney, NSW-2052, Australia*
[3]*Department of Physics, Chemistry and Biology (IFM), Linköping University Linköping, S-581 83, Sweden*
[4]*National Physical Laboratory, Teddington, TW11 0LW, United Kingdom*
[5]*Department of Physics, Royal Holloway, University of London, Egham, TW20 0EX, United Kingdom*
[6]*Department of Physics and Astronomy, Seoul National University, Seoul 151-747, South Korea*

(Received 29 May 2015; accepted 3 August 2015; published online 11 August 2015)

We investigate Ti/Au contacts to monolayer epitaxial graphene on SiC (0001) for applications in quantum resistance metrology. Using three-terminal measurements in the quantum Hall regime we observed variations in contact resistances ranging from a minimal value of 0.6 Ω up to 11 kΩ. We identify a major source of high-resistance contacts to be due bilayer graphene interruptions to the quantum Hall current, whilst discarding the effects of interface cleanliness and contact geometry for our fabricated devices. Moreover, we experimentally demonstrate methods to improve the reproducibility of low resistance contacts (< 10 Ω) suitable for high precision quantum resistance metrology. [http://dx.doi.org/10.1063/1.4928653]

Epitaxial graphene, grown by thermal decomposition of silicon carbide (SiC/G), displays a remarkable performance as a quantum resistance standard,[1,2] utilizing the half-integer quantum Hall effect (hiQHE) in this material (Figure 1(a),1(b)). The quantum Hall effect (QHE),[3] arising from Landau quantization in two-dimensional systems at low temperatures in strong magnetic fields, entails the vanishing of the longitudinal resistance and the quantization of transversal resistivity in rational fractions of the von Klitzing constant $R_K = h/e^2 \approx (25.8\ k\Omega)$, where h is the Planck's constant and e is the elementary charge. Owing to the fact that a resistance measurement gives access to fundamental constants, the quantum Hall effect has been officially used in resistance metrology to define the ohm since 1990.[4]

The observation of the quantum Hall effect in graphene presented exciting new opportunities for metrology,[1,5] since the unique electronic structure of graphene leads to an exceptionally robust QHE, observable even at room temperature.[6] In a recent direct comparison experiment between SiC/G and GaAs (the present system of choice for QHR),[2] the QHR was found to agree with a relative uncertainty of 10^{-10}. The accuracy of this comparison was limited by the lower breakdown current in the GaAs device (i.e. the maximum current that the material can sustain before quantum Hall vanishes), since this was an order of magnitude lower than what is achievable in SiC/G.[7] Together with opportunities to measure at relatively low fields,[8] SiC/G represents a very promising platform for QHR standards with robust performance and high precision.

[a]Authors to whom correspondence should be addressed. Electronic addresses: yager@chalmers.se and ywpark@snu.ac.kr

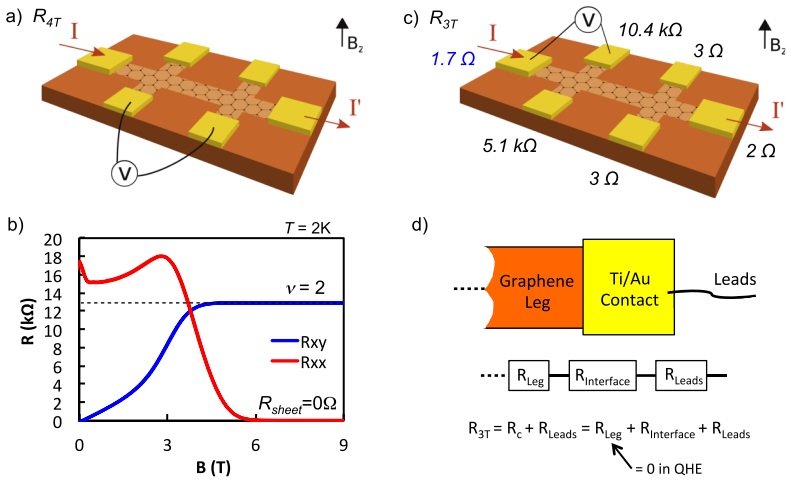

FIG. 1. Measurement setup illustrating three- and four-terminal resistance measurements in the quantum Hall regime. a) Schematic of a four-terminal resistance measurement on a 6 legged graphene Hall bar. b) Example of longitudinal (red) and transverse (blue) resistances as a function of magnetic field for a typical graphene device measured at 2 K. At high fields, the longitudinal resistance is equal to zero. c) Three-terminal resistance measurements can be adapted to exclude the von Klitzing resistance, to give a direct measurement of the contact resistance (plus the access resistance from cryostat leads). Resistance values represent a residue-free contacted device where the measured three-terminal contact resistances showed a local geometric spread from 2 Ω to 10.4 kΩ. (Blue shows measured value for the illustrated configuration, whilst black values show the equivalent three-terminal resistance at each other contact of the device) d) Schematics illustrating the series contributions to the contact resistance of the metal-graphene interface, lead resistance and the graphene 'leg' (=0 in QHE).

A major practical limitation to the performance of QHR standards are finite contact resistances (R_c). Under quantizing conditions, high resistance contacts contribute to thermal excitation of electrons to higher Landau levels by Joule heating, leading to high uncertainty in metrological measurements of R_K.[9] For GaAs heterostructures with alloyed AuGeNi contacts, it has been shown that high contact resistance values in the ~kΩ range translate into deviations of the measured quantum Hall resistance from $R_K/2$ up to 1 part per million.[10] Conversely, deviations can be <1 part per billion, if the resistance of the voltage contacts is below 100 Ω.[11] For SiC/G, it has been shown that ohmic contacts with $R_c < 10$ Ω can, in principle, be fabricated by standard lift-off technique using Ti/Au as a contact material.[12] However, in practice contacts with high resistance can be found even within the same device (Figure 1(c)). Similar on-device variations have been reported for GaAs, with their origin attributed to the disorder introduced by annealed contacts, which leads to inhomogeneous doping profiles around the metallic contacts.[13] As for graphene-based QHR standards, the problem of contact resistance variability has yet to be reported.

The established method to investigate contact resistance in a QHR device is to use three-terminal measurements.[10] These measurements comprise current injection from source to drain (I_{SD}), and measurement of the voltage between a third electrode and the drain contact (Figure 1(c)). In this configuration, the resulting three-terminal resistance includes the sum of the known lead resistance (R_{Leads}) and the contact resistance (R_c). For a typical Hall bar geometry the contact resistance comprises of both the metal-graphene interface resistance ($R_{Interface}$) plus the resistance of the graphene 'leg' (R_{Leg}) (Figure 1(d)). In the quantum Hall regime, both the channel resistance (R_{xx}) and the leg resistance vanish ($R_{xx}, R_{Leg} = 0$), and the three-terminal measurement can therefore yield a high-accuracy measurement of the metal-graphene interface resistance in geometrically independent units (Ω).[14] The method described contrasts with the commonly used transfer length method (TLM) for assessing contact resistance that typically yields a one-dimensional contact resistivity value for metallic graphene devices.[15–21] This method is unsuitable for assessing quantum Hall bar devices, since it is geometrically incompatible and can also lead to large measurement uncertainty for low charge carrier densities.[15]

In this study we investigate contact resistance in epitaxial graphene Hall bar devices for applications in quantum resistance metrology. We find that the Ti/Au-graphene system results in ohmic

contacts with variations in R_c, regardless of interface cleanliness, ranging from a minimal value of 0.6 Ω up to 11 kΩ. This variability can be explained by microscopic inhomogeneity of the epitaxial graphene material, and careful engineering of devices suppresses variability and ensures low R_c in all contacts.

The devices under study are Hall bars fabricated on 4 chips (7×7 mm^2) of epitaxial graphene grown on 4H-SiC (0001) at T = 2000 ºC and P = 1 atm Ar.[22,23] In order to achieve quantum Hall conditions, the graphene carrier density has been adjusted by photochemical gating.[24,25] Electron concentration for gated devices at 2 K was typically measured to be $n = (1.5 - 4) \times 10^{11}$ cm^{-2}. The fabricated 6-leg Hall bars (Figure 1(a)) have widths, w = 4, 8, 24 and 40 μm, equal to the metal-graphene contact edge perimeters, while the length/width ratio is kept constant to 7.5. We have fabricated devices following two approaches: 1) Hall bars fabricated by standard electron beam lithography (EBL), where organic resist residues from EBL at the metal-graphene contact interface were not fully removed[1,26] and 2) Hall bars with ultra-clean metal-graphene interface. Fabrication of Hall bars by EBL includes three steps: i) metallic anchors on SiC for electric contacts to graphene, ii) ohmic contacts to graphene (Figure 2(a)) and iii) selective removal of graphene to define structures (Figure S1).[27,28] Metallic contacts directly deposited on graphene are prone to detach upon wire bonding. For this reason, metallic anchors (5 nm Ti/ 70 nm Au) that provide strong adhesion to the substrate are deposited first directly on SiC (by removing graphene using oxygen plasma etching), and subsequently the actual electrical contacts to graphene are deposited (5 nm Ti/ 120 nm Au) in a second lithography step. The final step is to pattern the Hall bar using EBL with positive resist followed by oxygen plasma etching. As a result of this fabrication method, the metal-graphene interface is very likely to contain resist residues as shown on AFM images taken on the graphene surface just before deposition of electrical contacts (Figure 2(a)). On two other samples, an ultra-clean metal-graphene interface was ensured by avoiding the initial use of polymer resist. First, electrical contacts to graphene were deposited through a shadow mask (50 μm-thick silicon wafer) on a pristine SiC/G chip, free of organic contaminants (Figure 2(b)). Once a clean metal-graphene interface was formed, subsequent lithography steps (formation of anchors and defining Hall bars on graphene) were carried out using standard EBL with positive resists.

In order to investigate the effect of organic residues at the Ti/Au-graphene interface as a source of R_c variability we compared contacts, prepared by shadow mask evaporation and by standard

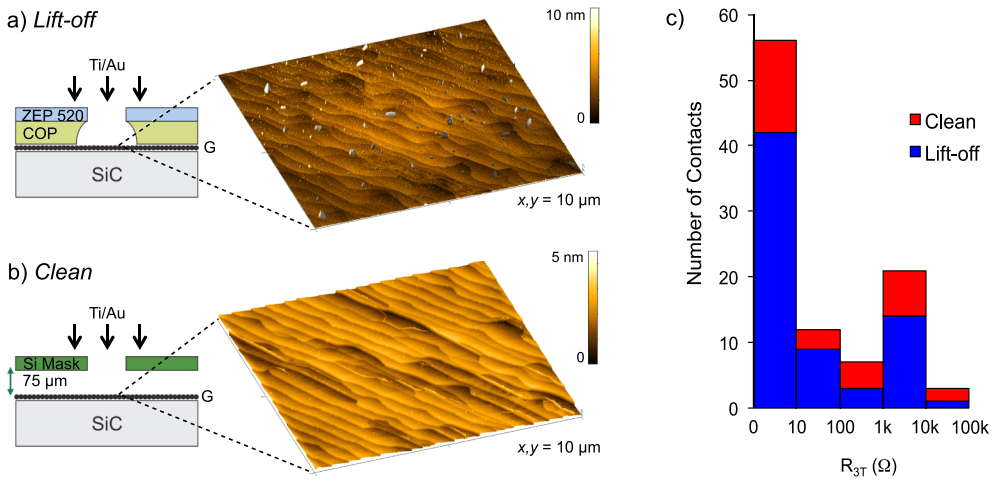

FIG. 2. Comparison between standard lift-off and ultra-clean electrical contact interfaces. a) Fabrication of contacts to SiC/G Hall bars by EBL includes the deposition of metallic anchors directly on SiC by removing graphene with oxygen plasma etching, followed by a second lithography step to provide electrical contact to graphene. b) Contact deposition through a 50 μm-thick silicon shadow mask enables an ultra-clean metal-graphene interface. AFM topographical images illustrate the contrast in cleanliness between graphene surfaces immediately before metal contact deposition by standard lithography or with a shadow mask, with RMS roughness equal to 1.8 nm and 0.5 nm respectively. c) Contact resistance statistics for 97 individual contacts measured by three-terminal resistance under quantum Hall conditions. The majority of contacts are below 10 Ω, however a spread in contact resistance is observed, even for devices fabricated with clean metal-graphene interfaces.

lithography, using three-terminal resistance measurements (R_{3T}) under quantum Hall conditions. A histogram summarizing the data collected for 97 contacts is shown in Figure 2(c). Both standard and ultra-clean fabricated contacts are ohmic with the majority displaying resistances below 10 Ω, suitable for metrology, with the best contact resistances found to be as low as 0.6 Ω. Nonetheless, we have also observed a significant abundance of high resistance contacts. The spread in contact resistances was observed for contacts fabricated using both a physical mask and by standard EBL. Moreover, a significant distribution of measured contact resistance was observed even within a single device (Figure 1(c)), where both fabrication conditions and the degree of contamination by resist residues can be assumed to be nominally identical. For these reasons, we discard the cleanliness of the metal-graphene interfaces as the source of high resistances in our three-terminal measurements.

In addition to the cleanliness of the metal-graphene interface, we have investigated the effects of varying the contact geometry and the thickness of the titanium contact adhesion layer. The contact geometry was varied for both clean and standard EBL fabricated contacts with overlap areas ranging from $(8 - 50) \times 10^3$ μm^2 and metal-graphene contact edge widths in the range of 4 - 40 μm. The thickness of the titanium contact adhesion layer varied between 0.5 - 5 nm for clean graphene surfaces. We found no significant trends relating either parameter to the minimum achieved contact resistance or to the abundance of high contact resistances within the range of parameters investigated (Figure S2).[28] For this reason we refrain from quantifying the specific contact resistivity,[19] as would be the case for contacts to metallic graphene, making a direct comparison to literature values measured outside of the quantum Hall regime less trivial.

In order to understand the variations in measured three-terminal resistances we recall that, for our standard Hall bar geometries, the effective contact includes contributions not only from the metal-graphene interface but also from the graphene leg (see Figure 1(d)). In the quantum Hall regime this sheet resistance contribution is exactly zero, however, in the case of an electronically inhomogeneous material, this assumption may not be valid. It has been demonstrated that purely monolayer Hall bar devices fabricated on our SiC/G show a very tight spread in charge carrier density and mobility across wafer scale dimensions.[29] In contrast, SiC/G devices containing bilayer graphene domains display variations in their electrical properties linked to the amount of bilayer content. Due to the semi-conducting nature[30] of Bernal stacked bilayer graphene that grows on SiC,[31–33] these bilayer regions are typically either metallic or insulating depending on the charge carrier density. Furthermore, it has been shown that a continuous bilayer patch spanning the width of a Hall bar leads to a locally non-vanishing quantum Hall sheet resistance, □ in either the metallic or insulating state.[34,35] In the context of this investigation, such inhomogeneities in the region of the Hall bar legs could account for the statistical abundance of locally high resistance contacts (Figure 1(c), 2(c)).

To investigate the hypothesis of bilayer graphene inhomogeneities as a major source of high contact resistance in the quantum Hall regime, we used express optical microscopy[34] together with high resolution large area Kelvin probe force microscopy (KPFM)[36,37] (Figure 3(a)). In KPFM, domains of monolayer and bilayer graphene are identified by the difference in their surface potentials.[38] An electrically characterized Hall bar device (channel width 24 μm) was selected for analysis due to wide variations in the measured resistance for each contact (values represented in Figure 1(c)). The graphene device surface was first cleaned free of polymer resist residues using contact mode AFM, since organic contaminants act to obscure the potential landscape and reduce measured contrast.[39] The characterized device contained a significant proportion (> 15%) of micron scale bilayer graphene patches. For the case where a continuous bilayer domain spanned the full width of the graphene leg (Figure 3(a)), we found that three-terminal contact measurements also yielded a high resistance (~kΩ).

In contrast, for device legs demonstrating low contact resistance, we observed the presence of uninterrupted monolayer graphene percolation paths around bilayer graphene inclusions. Such monolayer paths are found to allow dissipationless current to flow from the metal contact to the Hall bar channel, translating into low three-terminal resistance measurements. This underlines that it is the exact geometry of bilayer domains rather than simply their presence that leads to current dissipation in the monolayer QHR (Figure 3(b)). In the context of quantum resistance metrology it

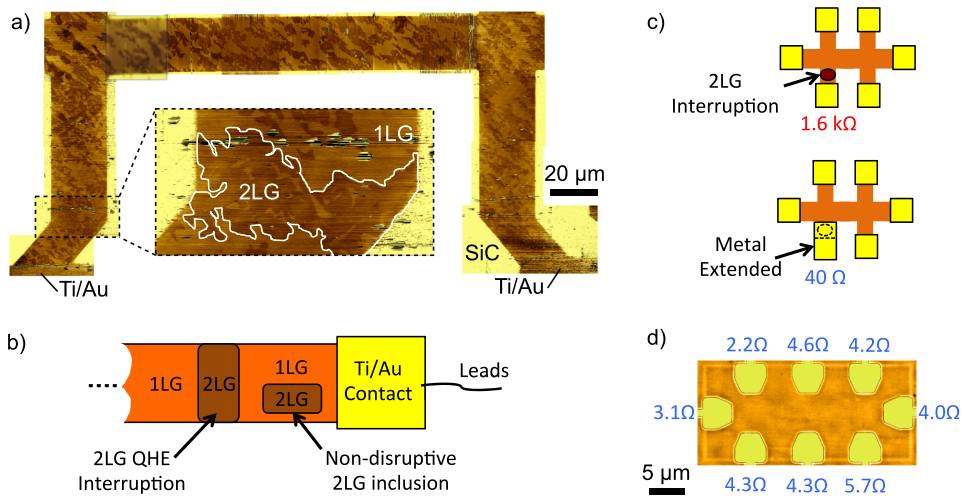

FIG. 3. a) Surface potential image of sections of a graphene Hall bar obtained by Kelvin probe force microscopy; in these images, monolayer graphene appears brighter than bilayer graphene. On the left leg, a bilayer patch stretches from one edge to the other (2LG dark color, 5 kΩ contact resistance), while on the right leg a percolation path for edge mode current flow exists to the metal contact (1LG graphene bright color, 2 Ω contact resistance). b) Schematic illustrating the resistance contributions in an epitaxial graphene Hall device as measured in the three-terminal geometry. The presence of bilayer graphene patches results in a geometrically dependant resistance additionally to the monolayer graphene component. c) Schematic diagram of a measured graphene Hall bar. The dark ellipse represents a bilayer patch at the voltage leg, leading to a high contact resistance measurement in QHR. When the metal contact was extended (right schematic), the measured contact resistance was reduced from 1.6 kΩ to 40 Ω. d) Optical transmission image of a 15 µm x 30 µm rectangular Hall bar with digital enhancement. The device is predominantly monolayer (light contrast) with micron scale bilayer inclusions (dark contrast). The bright rectangular border shows where graphene outline was defined by etching during fabrication. The colour of Ti/Au contacts is enhanced for additional contrast. The figure shows an example of consistently low resistances for all contacts in this measured device.

is highly important to avoid interruptions at the Hall bar legs since this contributes to the contact resistance ($R_c = R_{Interface} + R_{Leg}$) and can prevent accurate resistance quantization .

We demonstrate two approaches to eliminate the high resistance contributions originating from bilayer graphene domains in our devices. Firstly, in order to improve existing devices that originally display high three-terminal resistance, the metallized contact region can be re-deposited by EBL to extend towards the Hall channel, thus shunting the bilayer graphene inclusion. As an example, we found that electrically bypassing bilayer graphene inhomogeneities in this way reduced the measured three-terminal resistance from R_{3T} = 1.6 kΩ down to 40 Ω after this metal extension. Since this solution requires exact prior knowledge of the bilayer graphene geometry as well as additional fabrication and lithography steps, we have instead chosen to focus on improving the initial yield of graphene quantum Hall devices as outlined below.

The second approach involves engineering the geometry of Hall bars with built-in tolerances to the inherent bilayer stripe inhomogeneities in epitaxial graphene. In order to achieve this, prospective samples were pre-screened by means of express optical microscopy to quantify the amount of bilayer graphene coverage and those with the highest content of bilayer domains graphene (> 10%) were discarded.[34] In addition, we employ this microscopy technique to align the orientation of our devices with respect to bilayer stripe inhomogeneities that grow anisotropically along the silicon carbide terrace edges. Based on this approach, we fabricated wide rectangular Hall bars without graphene leg constrictions on pre-screened monolayer graphene, oriented in parallel to bilayer graphene stripes. (Figure 3(d)). These devices were fabricated by standard EBL (i.e. unclean metal-graphene interface) with Ti/Au (5 nm/75 nm) electrical contacts to graphene as described above (Figure 2(a)). Despite the relatively small metal-graphene contact geometry when compared to contacts summarized in Figure 2(c) (perimeter length w = 10 µm and contact area A = 25 µm^2), all eight contact resistances obtained from three-terminal measurements for the device are below 10 Ω, suitable for applications in quantum resistance metrology.

In summary, we have investigated the contact resistance of Ti/Au contacts to epitaxial graphene Hall bar devices by three-terminal measurements in the quantum Hall regime. The observed spread in resistance was found to originate from bilayer graphene interruptions at the Hall bar legs that locally disrupt the monolayer quantum Hall current. We have demonstrated methods to improve the reproducibility of low resistance Ti/Au-SiC/G contacts for quantum Hall resistance metrology using standard lithography, and shown that a contact area of the order of tens of μm^2 results in contact resistance $< 10\ \Omega$ provided that the geometry of Hall bars is properly engineered.

ACKNOWLEDGEMENTS

This work was partly supported by The Graphene Flagship (Contract No. CNECT-ICT-604391), Swedish Foundation for Strategic Research (SSF), Linnaeus Centre for Quantum Engineering, Knut and Alice Wallenberg Foundation, Chalmers AoA Nano, the Swedish-Korean Basic Research Cooperative Program (No. 2014R1A2A1A1 2067266) of the NRF, and the EMRP project GraphOhm. The EMRP is jointly funded by the EMRP participating countries within EURAMET and the European Union. T.Y. is grateful to J. Kosmaca for stimulating discussions.

[1] A. Tzalenchuk, S. Lara-Avila, A. Kalaboukhov, S. Paolillo, M. Syväjärvi, R. Yakimova, O. Kazakova, T.J.B.M. Janssen, V. Fal'ko, and S. Kubatkin, Nat. Nanotechnol. **5**, 186 (2010).
[2] T.J.B.M. Janssen, J.M. Williams, N.E. Fletcher, R. Goebel, A. Tzalenchuk, R. Yakimova, S. Lara-Avila, S. Kubatkin, and V.I. Fal'ko, Metrologia **49**, 294 (2013).
[3] K. v. Klitzing, G. Dorda, and M. Pepper, Phys. Rev. Lett. **45**, 494 (1980).
[4] B.N. Taylor, IEEE Trans. Instrum. Meas. **39**, 2 (1990).
[5] A.J.M. Giesbers, G. Rietveld, E. Houtzager, U. Zeitler, R. Yang, K.S. Novoselov, A.K. Geim, and J.C. Maan, Appl. Phys. Lett. **93** (2008).
[6] K.S. Novoselov, Z. Jiang, Y. Zhang, S. V Morozov, H.L. Stormer, U. Zeitler, J.C. Maan, G.S. Boebinger, P. Kim, and A.K. Geim, Science **315**(80), 1379 (2007).
[7] J.A. Alexander-Webber, A.M.R. Baker, T.J.B.M. Janssen, A. Tzalenchuk, S. Lara-Avila, S. Kubatkin, R. Yakimova, B.A. Piot, D.K. Maude, and R.J. Nicholas, Phys. Rev. Lett. **111**, 96601 (2013).
[8] A. Satrapinski, S. Novikov, and N. Lebedeva, Appl. Phys. Lett. **103**, 173509 (2013).
[9] I.I. Kaya, G. Nachtwei, K. von Klitzing, and K. Eberl, Europhys. Lett. **46**, 62 (1999).
[10] F. Delahaye and B. Jeckelmann, Metrologia **40**, 217 (2003).
[11] B. Jeckelmann, B. Jeanneret, and D. Inglis, Phys. Rev. B **55**, 13124 (1997).
[12] A. Tzalenchuk, S. Lara-Avila, A. Kalaboukhov, S. Paolillo, M. Syväjärvi, R. Yakimova, O. Kazakova, T.J.B.M. Janssen, V. Fal'ko, and S. Kubatkin, Nat. Nanotechnol. **5**, 186 (2010).
[13] F. Dahlem, E. Ahlswede, J. Weis, and K. v. Klitzing, Phys. Rev. B **82**, 121305 (2010).
[14] U. Klass, W. Dietsche, K. Von Klitzing, and K. Ploog, Zeitschrift Für Phys. B Condens. Matter **82**, 351 (1991).
[15] F. Xia, V. Perebeinos, Y. Lin, Y. Wu, and P. Avouris, Nat. Nanotechnol. **6**, 179 (2011).
[16] B.C. Huang, M. Zhang, Y. Wang, and J. Woo, Appl. Phys. Lett. **99**, 032107 (2011).
[17] V.K. Nagareddy, I.P. Nikitina, D.K. Gaskill, J.L. Tedesco, R.L. Myers-Ward, C.R. Eddy, J.P. Goss, N.G. Wright, and A.B. Horsfall, Appl. Phys. Lett. **99**, 073506 (2011).
[18] A. Venugopal, L. Colombo, and E.M. Vogel, Appl. Phys. Lett. **96**, 013512 (2010).
[19] K. Nagashio, T. Nishimura, K. Kita, and a. Toriumi, Appl. Phys. Lett. **97**, 143514 (2010).
[20] J. Robinson, M. LaBella, M. Zhu, M. Hollander, R. Kasarda, Z. Hughes, K. Trumbull, R. Cavalero, and D. Snyder, Appl. Phys. Lett. **98**, 053103 (2011).
[21] S. Russo, M.F. Craciun, M. Yamamoto, a. F. Morpurgo, and S. Tarucha, Phys. E Low-Dimensional Syst. Nanostructures **42**, 677 (2010).
[22] R. Yakimova, T. Iakimov, and M. Syväjärvi, PCT/SE2011/050328 (2011).
[23] C. Virojanadara, M. Syväjarvi, R. Yakimova, L. Johansson, A.A. Zakharov, and T. Balasubramanian, Phys. Rev. B **78**, 1 (2008).
[24] S. Lara-Avila, K. Moth-Poulsen, R. Yakimova, T. Bjørnholm, V. Fal'ko, A. Tzalenchuk, and S. Kubatkin, Adv. Mater. **23**, 878 (2011).
[25] A. Tzalenchuk, S. Lara-Avila, K. Cedergren, M. Syväjärvi, R. Yakimova, O. Kazakova, T.J.B.M. Janssen, K. Moth-Poulsen, T. Bjørnholm, S. Kopylov, V. Fal'ko, and S. Kubatkin, Solid State Commun. **151**, 1094 (2011).
[26] T. Yager, M.J. Webb, H. Grennberg, R. Yakimova, S. Lara-Avila, and S. Kubatkin, Appl. Phys. Lett. **106** (2015).
[27] S. Lara-Avila, *Magnetotransport Characterization of Epitaxial Graphene on SiC* (Department of Microtechnology and Nanoscience, Quantum Device Physics, Chalmers University of Technology, 2012).
[28] See supplementary material at http://dx.doi.org/10.1063/1.4928653 for Details of Sample Fabrication and Geometry and Ti Thickness Dependence of the Contact Resistance.
[29] T. Yager, A. Lartsev, R. Yakimova, S. Lara-Avila, and S. Kubatkin, Carbon **87**, 409 (2015).
[30] E. McCann, Phys. Rev. B **74**, 161403 (2006).
[31] T. Ohta, A. Bostwick, T. Seyller, K. Horn, and E. Rotenberg, Science **313**, 951 (2006).
[32] C. Coletti, C. Riedl, D.S. Lee, B. Krauss, L. Patthey, K. von Klitzing, J.H. Smet, and U. Starke, Phys. Rev. B **81**, 235401 (2010).

[33] L.O. Nyakiti, R.L. Myers-Ward, V.D. Wheeler, E.A. Imhoff, F.J. Bezares, H. Chun, J.D. Caldwell, A.L. Friedman, B.R. Matis, J.W. Baldwin, P.M. Campbell, J.C. Culbertson, C.R. Eddy, G.G. Jernigan, and D.K. Gaskill, Nano Lett. **12**, 1749 (2012).
[34] T. Yager, A. Lartsev, S. Mahashabde, S. Charpentier, D. Davidovikj, A. V Danilov, R. Yakimova, V. Panchal, O. Kazakova, A. Tzalenchuk, S. Lara-Avila, and S. Kubatkin, Nano Lett. **13**, 4217 (2013).
[35] C. Chua, M. Connolly, A. Lartsev, T. Yager, S. Lara-Avila, S. Kubatkin, S. Kopylov, V. Fal'Ko, R. Yakimova, R. Pearce, T.J.B.M. Janssen, A. Tzalenchuk, and C.G. Smith, Nano Lett. **14**, 3369 (2014).
[36] T. Burnett, R. Yakimova, and O. Kazakova, Nano Lett. **11**, 2324 (2011).
[37] T. Burnett, R. Yakimova, and O. Kazakova, J. Appl. Phys. **112**, 54307 (2012).
[38] V. Panchal, R. Pearce, R. Yakimova, A. Tzalenchuk, and O. Kazakova, Sci. Rep. **3**, 2597 (2013).
[39] N. Lindvall, A. Kalabukhov, and A. Yurgens, J. Appl. Phys. **111** (2012).